Available online at www.sciencedirect.com

ScienceDirect

journal homepage: www.elsevier.com/locate/he

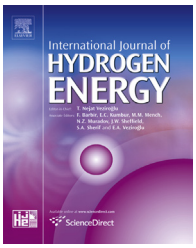

Sizing methodology for hybrid systems based on multiple renewable power sources integrated to the energy management strategy

Diego Feroldi[*], *David Zumoffen*[1]

French-Argentine International Center for Information and Systems Sciences (CIFASIS-CONICET-UNR-AMU), 27 de Febrero 210 bis, S2000EZP Rosario, Argentina

ARTICLE INFO

Article history:
Received 5 August 2013
Received in revised form
16 December 2013
Accepted 3 January 2014
Available online 1 February 2014

Keywords:
Renewable energy sources
Bioethanol
System sizing
Energy management strategy
PEM fuel cells
Stand alone power systems

ABSTRACT

This work presents a design methodology for a hybrid energy system based on multiple renewable power sources and bioethanol. The new concept of generation consists on having multiple power sources such as a PEM fuel cell system fed by the hydrogen produced by a bioethanol reformer and wind-solar sources working all together supervised by the energy management system. The necessary heating for the bioethanol reforming reaction can be provided by the renewable sources to enhance the efficiency of the hydrogen production. It is worth noting that, from the power balance as well as backup point of views, the hybrid system is equipped with energy storage devices. An optimal sizing methodology integrated with the energy management strategy is proposed here for designing the overall hybrid system. The suggested approach is based on genetic algorithms, using historical climate data and load demands over a period of one year. Several simulation results are given to show the methodology performance in terms of loss of power supply probability (**LPSP**), costs and bioethanol consumption.

1. Introduction

Currently, there is a growing concern for the environment based primarily on the climate change and desertification caused by the large amounts of CO_2 emissions into the atmosphere. In this context, the use of renewable energies can contribute to alleviate these situations. Moreover, the production of biodiesel and bioethanol is expanding as a result of measures to encourage the change of the energy matrix, making it less dependent on fossil fuels.

Renewable energy sources have a lot of advantages including sustainability, low pollution and economic benefits. However, due to the intermittent nature of many renewable resources, it is necessary to combine more than one source for a reliable system, constituting a hybrid system based on renewable energy sources. For instance, wind and solar energy in a given area can be complementary in a certain period of time. However, in order to meet the load requirements in stand-alone applications, it is also necessary to incorporate some kind of energy storage. The use of batteries with high specific energy is continuously rising, although storing large

* *Corresponding author*. Universidad Nacional de Rosario – FCEyA, Pellegrini 250, S2000BTP Rosario, Argentina. Tel.: +54 341 4237248 304; fax: +54 341 482 1772.
E-mail addresses: feroldi@cifasis-conicet.gov.ar, dferoldi@gmail.com (D. Feroldi), zumoffen@cifasis-conicet.gov.ar (D. Zumoffen).
[1] Universidad Tecnológica Nacional – FRRo, Zeballos 1341, S2000BQA Rosario, Argentina. Tel.: +54 341 4237248 304; fax: +54 341 482 1772.

0360-3199/$ – see front matter
http://dx.doi.org/10.1016/j.ijhydene.2014.01.003

amounts of energy may not be feasible. Therefore, the use of other energy source to act as a backup for the wind-solar system is necessary to achieve a reliable system that can feed an isolated load for a wide range of weather conditions. In this sense, a PEM (Polymer Electrolyte Membrane) fuel cell together with a bioethanol reformer, to produce hydrogen from bioethanol, can provide a power supply for a long time in an environmentally friendly way.

In view of the foregoing, this paper deals with a new concept of hybrid system with multiple sources to ensure a reliable and efficient power supply. The system consist of renewable energy sources (wind and solar) and hydrogen production from bioethanol. The bioethanol reformer produces hydrogen with sufficient quality to feed a PEM fuel cell. This fuel cell can in turn power the load. The load can also be powered from wind turbines, an array of photovoltaic panels (PV), and a battery bank.

In the present paper, a new methodology for the design of hybrid systems with multiple sources is addressed. The design methodology is based on historical data (meteorological and power consumption data) and it is integrated with the energy management strategy (EMS). The EMS is an algorithm capable of commanding in real time the energy sources involved in order to meet the load requirements in an efficient and secure manner [1].

The organization of this paper is as follows. In Section 2 a detailed description of the power generation system is performed. Section 3 deals with the energy management strategy used to manage the flow of energy within the designed system. Section 4 deals with the component sizing of the hybrid renewable energy system. In Section 5, the obtained results are presented and discussed. Finally, in Section 6 the conclusions are stated.

2. Description of the system

This section describes the hybrid power system and also addresses the modeling of the different parts. The topology of the system under study in this work is shown in Fig. 1. This figure shows how the load power is supplied by the PEM fuel cell, the wind turbine and the PV array. The battery bank can also provide power to the DC bus when necessary. It further notes that the reformer heater can be fed, at least partially, with power from the DC bus. The power from the sources can be fully sent to the load, but if required, it can be partially sent to the battery bank to be stored temporarily and used a posteriori according to the demand. The power from the sources can be also sent to the heater of the bioethanol reformer when it is necessary to turn on the PEM fuel cell. A proper energy management strategy is responsible of commanding this operation, which is explained in detail in Section 3.

The power balance in the DC bus in Fig. 1 can be expressed as follows:

$$P_L(t) = \eta_{DA}(\eta_{AD}P_w(t) + \eta_{DD}P_{PV}(t) + \eta_{DD}P_{FC}(t) + \eta_{DD}P_b(t) - P_h(t)), \quad (1)$$

where $P_w(t)$, $P_{PV}(t)$, $P_{FC}(t)$, and $P_b(t)$ are the power provided by the wind turbines, the PV array, and the fuel cells, and the battery bank, respectively, and $P_h(t)$ is the power consumed by the heater in the reformer. The constants η_{DD}, η_{AD}, and η_{DA} are the efficiencies of the DC/DC, the AC/DC, and the DC/AC power converter, respectively. These efficiencies are assumed to be constant, being $\eta_{DD} = 0.95$ and $\eta_{AD} = \eta_{DA} = 0.9$. On the other hand, $P_b(t)$ is negative by convention when the battery bank is charging and positive when is discharging.

Due to physical and operative limitations, the power balance is subjected to the following constraints:

$$\begin{array}{ccccc} 0 & \leq & P_w(t) & \leq & P_w^{av}(t) \\ 0 & \leq & P_{PV}(t) & \leq & P_{PV}^{av}(t) \\ P_{FC}^{min} & \leq & P_{FC}(t) & \leq & P_{FC}^{max} \\ \Delta P_{FC}^{min} & \leq & \Delta P_{FC}(t) & \leq & \Delta P_{FC}^{max} \\ P_b^{min} & \leq & P_b(t) & \leq & P_b^{max} \end{array} \quad (2)$$

where $P_w^{av}(t)$ is the available power from the wind turbines; $P_{PV}^{av}(t)$ is the available power generation from the PV array; P_{FC}^{min} and P_{FC}^{max} are the minimum and maximum fuel cells power, respectively; ΔP_{FC}^{min} and ΔP_{FC}^{max} are the maximum fuel cells power fall rate and power rise rate, respectively; P_b^{min} and P_b^{max} are the minimum and maximum battery bank power.

2.1. Wind turbines

The mechanical power captured by a wind turbine is proportional to the swept blade area (A), the air density (ρ_a), the wind velocity (v) and the coefficient of power (C_P), which expresses

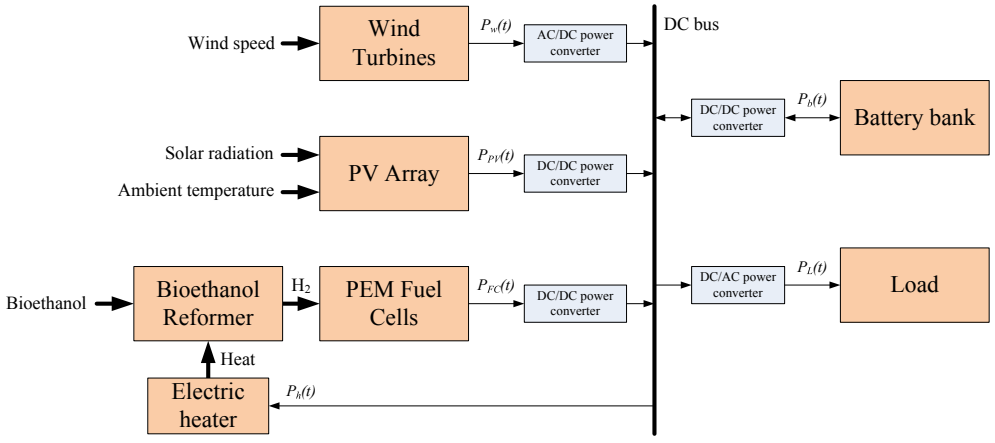

Fig. 1 – Schematic diagram of the hybrid generation system based on renewable sources and bioethanol.

the efficiency of the turbine as a function of the ratio λ defined as $\lambda = r\omega_m/v$, where r is the radius of the blades and ω_m is the speed angle of the turbine shaft [2]. The ratio C_p, depending on λ and the blade pitch angle β, can be expressed as [3]:

$$C_p(\lambda,\beta) = \frac{1}{2}\left(\frac{rC_f}{\lambda} - 0.022\beta - 2\right)e^{-0.255\frac{rC_f}{\lambda}}, \quad (3)$$

where C_f is a design constant of the blades. The values of the parameters used are as follows: $\rho_a = 1.2$ kg m^3, $r = 1.84$ m, $A = 8$ m^2, $C_f = 19.92$. Therefore, the power from a wind turbine can be expressed as follows [2]:

$$P_w(t) = \frac{1}{2}C_p(\lambda,\beta)\rho_a A v^3(t). \quad (4)$$

However, this power is only possible for a certain range of wind speeds.

The wind turbine operation can be divided into two regions: i) above a rated wind speed $v_r = 9$ m s^{-1} (full load) and ii) below-rated wind speed (partial load) [4]. When the load is below the rated power P_w^r, the turbine operates at variable rotor speeds, fixing the blade pitch angle. For wind speeds above the rate value, the turbine is operated at constant output power, varying the blade pitch angle [5]. On the other hand, the wind turbine is stopped for wind speeds below a lower limit ($v_l = 5$ m s^{-1}) and above an upper limit ($v_u = 20$ m s^{-1}). Therefore, on the basis of the above and (4), the available power from a wind turbine as a function of the wind speed can be expressed as follows:

$$P_w^{av}(t) = \begin{cases} 0 & \text{if } v < v_l \\ \frac{1}{2}C_p(\lambda,\beta)\rho_a A v^3(t) & \text{if } v_l \le v \le v_r \\ P_w^r & \text{if } v_r < v \le v_u \\ 0 & \text{if } v > v_u \end{cases}. \quad (5)$$

2.2. PV array

The electric behavior of a PV cell can be modeled by a nonlinear current source connected in series with the intrinsic cell series resistance. The current provided by this equivalent nonlinear source (I_{PV}) depends mainly on the actual insolation and the temperature [6]:

$$I_{PV}(t) = I_{ph}(t) - I_{rs}(t)\left(\exp\left(\frac{q(V_{PV}(t) + I_{PV}(t)R_s)}{A_c KT(t)}\right) - 1\right), \quad (6)$$

where I_{ph} is the generated current under a given insolation, I_{rs} is the cell reverse saturation current, V_{PV} is the voltage level on the PV panel array terminals, q is the charge of an electron, R_s is the intrinsic cell resistance, A_c is the cell deviation from the ideal p-n junction characteristic, K is the Boltzman constant, and T is the cell temperature. The reverse saturation current and the photocurrent depend on insolation and temperature according to the following expressions:

$$I_{rs}(t) = I_{or}\left(\frac{T(t)}{T_{ref}}\right)^3 \exp\left(\frac{qE_{go}(1/T_r - 1/T(t))}{KT(t)}\right), \quad (7)$$

$$I_{ph}(t) = (I_{sc} + K_l(T(t) - T_r))\lambda(t)/100, \quad (8)$$

where I_{or} is the reverse saturation current at the reference temperature T_{ref}, E_{go} is the band-gap energy of the semiconductor used in the cell, I_{sc} is the short-circuit cell current at the reference temperature and isolation, K_l is the short-circuit current temperature coefficient and λ is the insolation in mW/cm^2. The values of these constants are given in Table 1.

A PV array is a group of several PV modules which are electrically connected in series and parallel circuits to generate the required current and voltage. Thus, the available current for a PV array can be expressed as follows:

$$I_{PV}^{av}(t) = n_p I_{ph}(t) - n_p I_{rs}(t)\left(\exp\left(\frac{q(V_{PV}(t) + I_{PV}(t)R_s)}{n_s A_c KT(t)}\right) - 1\right), \quad (9)$$

where n_p is the number of parallel modules, and n_s is the number of cells connected in series in each parallel module. Therefore, the available power generation from a PV array is

$$P_{PV}^{av}(t) = V_{PV}(t)I_{PV}^{av}(t), \quad (10)$$

where $V_{PV}(t)$ is the output voltage of the PV module.

2.3. PEM fuel cell

PEM fuel cells are electrochemical devices that produce electrical energy with high efficiency. In a basic fuel cell, there are two electrodes (anode and cathode) separated by an electrolyte composed of a polymeric membrane, which has the characteristic that it allows the passage of protons when the membrane is conveniently hydrated but, on the contrary, is an excellent insulator for electron [7]. The anode is fed with hydrogen, while the cathode is fed with air.

The rate of hydrogen consumed in the electrochemical reaction in the fuel cell anode is a function of the fuel cell current:

$$W_{H_2,rct} = \frac{M_{H_2} n_{FC}}{2F} I_{FC}, \quad (11)$$

where $W_{H_2,rct}$ is the rate of hydrogen reacted, $M_{H_2} = 2.016 \times 10^{-3}$ kg mol^{-1} is the molar mass of oxygen, n_{FC} is the number of cells in the stack, $F = 96485$ C mol^{-1} is the Faraday number, and I_{FC} is the stack current. This is the amount of hydrogen that is required to the bioethanol processor system presented in Section 2.4.

The hydrogen consumption map of a PEM fuel cell system clearly reveals a zone, below a limit power, where the efficiency is very poor, while the zone above this limit power has a significant higher efficiency [1]. Therefore, the PEM fuel cell system must be operated in this advantageous zone where the efficiency is high. The maximum power is limited by the rated power, whereas the minimum must be limited to a value

Table 1 – Parameters used in the solar system.

Parameter	Value
q	1.6×10^{-19} C
A_c	1.6
K	1.3805×10^{-23} NmK^{-1}
K_l	0.0017 AoC^{-1}
I_{or}	2.0793×10^{-6} A
T_{ref}	301.18 K
E_{go}	1.10 V

below which it is not suitable to operate because the parasitic load is too large, reducing the system net power:

$$P_{FC}^{min} \leq P_{FC}(t) \leq P_{FC}^{max}. \quad (12)$$

On the other hand, the fuel cell power can not be increased faster than a certain power rise rate (ΔP_{FC}^{max}) to avoid a lack of reactants and the power can not be decreased faster than a certain power fall rate (ΔP_{FC}^{min}) to prevent overpressure into the stack [1]:

$$\Delta P_{FC}^{min} \leq \Delta P_{FC}(t) \leq \Delta P_{FC}^{max}, \quad (13)$$

where $\Delta P_{FC}(t) = P_{FC}(t) - P_{FC}(t - \Delta T)$ and ΔT is the sample time. The main parameters of the fuel cell modules used in this paper are in Table 2.

2.4. Bioethanol reformer

The bioethanol reformer (BRS) system consists of an ethanol steam reformer (ESR), which performs most of the conversion of bioethanol to hydrogen, followed by two water–gas shift reactors (WGS) and a preferential oxidation reactor of CO (CO-PrOx) that perform the hydrogen cleaning [8]. In the first step to produce the decomposition of ethanol, the bioethanol is mixed with vaporized water, and then supplied to the ESR:

$$(ESR) \quad CH_3CH_2OH + 3H_2O \leftrightarrow 4H_2 + 2CO$$

The reaction produced in the WGS is as follows:

$$(WGS) \quad CO + H_2O \leftrightarrow CO_2 + H_2.$$

This reaction produces heat and more hydrogen.

After the two WGS (high-temperature shift (HTS) and low-temperature shift (LTS) reactors), the CO levels are still too high to fed a PEM fuel cell, so that the final elimination takes place in the CO-PrOx reactor where is produced CO oxidation. For this, air is injected into the CO-PrOx reactor to provide oxygen for the CO oxidation:

$$(CO - PrOx) \quad CO + \frac{1}{2}O_2 \leftrightarrow CO_2.$$

The ESR reaction is endothermic, thus it requires a heat supply. The amount of heat necessary to supply is $\Delta H_{298}^{o} = 254.8\ kJ\ mol^{-1}$. In the present work, it is proposed to provide this heat through a heating resistor, which is supplied with energy provided by a hybrid wind-solar system and part of the energy previously stored in the batteries. The heat transfer is achieved by passing the gases through the jacket of the reformer. Derived from the ESR reaction, the necessary power to supply the heater reformer is

$$P_H = \frac{W_{H_2,rct}\Delta H_{298}^{o}}{4}. \quad (14)$$

Table 2 – Parameters of the PEM fuel cell modules.

Parameter	Value
Type	PEM
Rated power	1.2 kW
Maximum rise rate power	60 W
Maximum fall rate power	−90 W

2.5. Energy storage system

Each battery in the energy storage system is modeled as an equivalent circuit comprising a voltage source, which represents the open circuit voltage (V_{oc}), in series with an internal resistance (R_{int}). Therefore, the terminal voltage of the battery is $V_{bat} = V_{oc} - I_{bat}R_{int}$. In this model, both V_{oc} and R_{int} depend on the battery state of charge (SOC_b), which represents the remaining capacity still available to be discharged from the battery. In the model, the nonlinear interactions of V_{oc} and R_{int} depending on SOC_b are expressed as data vectors and their values are obtained by interpolating within the corresponding vector according to the current SOC_b. These vectors are based on experimental data of the manufacturer and can be obtained from the modeling tool of hybrid automation systems called ADVISOR [9].

The SOC_b can be expressed as

$$SOC_b = \frac{C_b^{*,max} - C_b^{*,u}}{C_b^{*,max}} \cdot 100 \quad [\%], \quad (15)$$

where $C_b^{*,max}$ is the maximum capacity, in units of ampere-hour, and $C_b^{*,u}$ is the amount of ampere-hour already used, which can be computed as

$$C_b^{*,u} = \int_0^t \frac{\eta_c I_b}{3600}\, dt \quad [Ah], \quad (16)$$

where η_c is the charge/discharge battery Coulombic efficiency, in this case $\eta_c = 0.975$, and I_b is the battery current in units of A at the current instant, being $I_b > 0$ when the battery discharges and $I_b < 0$ when it charges. The initial SOC_b is represented using a non-zero initial value of $C_b^{*,u}$. The SOC_b must be kept within certain limits, $SOC_b^{min} \leq SOC_b \leq SOC_b^{max}$, to ensure good performance and battery life.

The battery current is also limited, where these limits depend on V_{oc} and R_{int} through the following expressions:

$$I_b^{lim} = \begin{cases} \frac{(V_{oc} - V_b^{max})}{R_{int}} & \text{during charging} \\ \frac{(V_{oc} - V_b^{min})}{R_{int}} & \text{during discharging} \end{cases}, \quad (17)$$

where V_b^{min} and V_b^{max} are the minimum and maximum allowable battery bank voltage, respectively. Additionally, I_b^{lim} depend indirectly on SOC_b through the previously mentioned nonlinear relationships. Furthermore, there is another mechanism for limiting the battery bank current in order to force a current zero when the SOC_b reaches its maximum or minimum value. Therefore, the limit battery power is $P_b^{lim}(t) = I_b^{lim}(t)V_b(t)$. The main characteristics of the battery bank are given in Table 3.

Table 3 – Parameters of the batteries.

Parameter	Value
Type battery	Lead-Acid
Nominal capacity of each battery	104 Ah
Nominal voltage	13 V
Minimum voltage	9.5 V
Maximum voltage	16.5 V

3. Energy management strategy

It is required to define an adequate energy management strategy (EMS) to command efficiently the hybrid generation system, i.e., to determine at each instant the operation of the wind turbine, the PV array, the PEM fuel cell, and the battery bank, depending on the load requirements, the SOC_b, and the atmospheric conditions. The EMS must ensure that the energy balance in (1) is met, subjected to the constraints in (2). Different approaches for addressing EMS in hybrid systems with multiple renewable energy sources are found in literature, depending on whether the application is stand-alone or grid-connected. In the first category, which is the case covered here, different approaches can be found such as supervisory control switching between operation modes [10,11] or supervisory control based on model predictive control [12]. A stand-alone PV-H_2 system with a double hysteresis control scheme is in Ref. [13]. Three EMS based on switching between different modes are presented and compared in Ref. [14], applied to a stand-alone power system based on a PV array and wind generators that stores the excessive energy in the form of hydrogen.

In the system addressed in this paper, the available power from the wind subsystem is $P_w^{av}(t) = i_w^{av}(t)V_{bus}(t)$ according to (5), while the available power from the solar subsystem is $P_{PV}^{av}(t) = i_{PV}^{av}(t)V_{bus}(t)$ according to (10). The available currents $i_{PV}^{av}(t)$ and $i_w^{av}(t)$ are defined according the input currents to the DC–DC converters (see Fig. 1) and the respective conversion ratios. The wind turbine, solar cells and the reformer-fuel cell are usually controlled by inner regulation loops. The dynamics of these loops are much faster than those of outer control loops. Therefore, the current of each power source is considered to follow its reference perfectly.

In the proposed EMS (similar to the presented in Ref. [15]), the main generation role is in charge of the wind subsystem while the solar subsystem plays a secondary role. The motivation for this criterion is because of the intended application is in geographical areas with wealthy wind regimes. Therefore, the first objective is that the proposed energy management strategy operates the wind turbine at its maximum power point so long as possible. Thus, the role of the solar subsystem is to reinforce the wind subsystem. Similarly, the battery bank also reinforces the wind-solar subsystems.

The proposed EMS can be formalized using a state machine approach. State machine is a powerful tool to implement decision making algorithms. It can be used both as a development tool for approaching and solving problems and as a formal way of describing the solution for later developers and system maintainers. In the state machine concept, the system makes a transition from one state (mode) to another, provided that the condition (event) defining the change is true [16]. In the proposed EMS, these states define a mode of operation of the hybrid system indicating how the generation/storage systems operate in each mode. Switching between modes is defined on the basis of events, which are defined from comparison rules using process variables (load power, powers available, state of charge of the batteries, etc.).

Thus, a state machine consists of state and events. The states represents the behaviors of the system and the events are the conditions that cause a change in the current state. A state machine can be represented by a statechart. The statechart representing the proposed EMS is given in Fig. 2, which can be defined by a tuple $\langle S, \Sigma, \delta \subseteq S \times \Sigma \times S, s_0 \rangle$, where

- $S = \{s_1, s_2, s_3, s_4, s_5\}$ is the set of all nodes in the statechart.
- $\Sigma = \{1, 2, 3, 4, 5, 6, 7, 8\}$ is the set of possible input events (defined in Table 4).
  - δ is a function that maps states and input events to states ($\delta : S \times \Sigma \rightarrow S$), which can be expressed in the form of a state/event table or a statechart as in Fig. 2.
- s_0 is the initial state, i.e., an element of S. In this case, $s_0 = s_1$.

The description of each state in the set S is the following:

- State 1 (s_1): When the wind power is sufficient to satisfy the total demand, the wind subsystem operates at maximum power (point of maximum energy conversion) to satisfy the demand, and recharge the battery bank with the remaining energy, while the solar subsystem is inactive. The battery bank demands the recharge current and becomes part of the demand.
- State 2 (s_2): When the wind subsystem is not capable of supporting the load by itself, the wind subsystem is set for maximum generation and the solar subsystem supplies the remaining power to satisfy the power balance. The battery bank is also in charging mode.
- State 3 (s_3): When the two power subsystem together are not capable to met the power requirement, they operate at their maximum energy conversion points and the battery bank supplies the remaining power to fully satisfy the load demand. Thus, in this mode, the battery bank reverts the current direction, acting as a power supplier and depleting the previously stored energy (discharging mode).
- State 4 (s_4): When the battery bank SOC_b reaches the maximum limit (SOC_b^{max}), the power sources are disconnected, and the battery bank operates in mode discharging, supplying the required load.
- State 5 (s_5): When the battery bank SOC_b reaches the minimum limit (SOC_b^{min}), the PEM fuel cell and the reformer are connected. The battery bank operates in mode charging if there is a surplus of power, allowing to recover the charge.

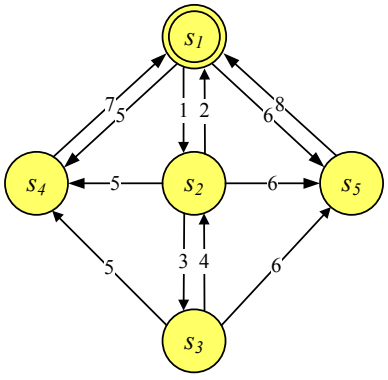

Fig. 2 – Schematic diagram of the energy management strategy (EMS).

Table 4 – Events in the set Σ.

Event	Description
1	$p_L^{req} > p_w^a$
2	$p_L^{req} < (p_w^a - \Delta p^{thr})$
3	$p_L^{req} > (p_w^a + p_{PV}^a)$
4	$p_L^{req} < (p_w^a + p_{PV}^a - \Delta p^{thr})$
5	$SOC_b \geq SOC_b^{max}$
6	$SOC_b \leq SOC_b^{min}$
7	$SOC_b < (SOC_b^{max} - \Delta SOC_b^{thr})$
8	$SOC_b > (SOC_b^{min} + \Delta SOC_b^{thr})$

4. Component sizing of the hybrid system

In a hybrid system with renewable sources the dimensioning process is crucial to ensure the power supply while remaining economically viable. The sizing of renewable hybrid systems is a complex issue because there is a compromise between cost and reliability, coupled with the uncertainty in demand and energy production, which depends on the weather conditions (wind speed, solar radiation, ambient temperature, etc.). Also, the sizing of the system is deeply related to the energy management strategy (EMS) used. Therefore, the main objectives in the design process can be stated as follows: (a) achieve a reliable power supply under varying atmospheric conditions and (b) minimize the total system cost. In standalone systems, the main priority is the reliability of the system [17].

The power reliability analysis is an important step in the component sizing process. *LPSP* is defined as the probability that the hybrid system is unable to satisfy the load demand [18]. Therefore, the main objective of component sizing is that $LPSP < LPSP_a$, where $LPSP_a$ is the allowed *LPSP*. The *LPSP* function can be expressed as follows:

$$LPSP = \frac{T_{ft}}{T_t}, \tag{18}$$

where T_t is the total time of weather data used in the analysis and T_{ft} is the power failure time, which is defined as the time that the load is not satisfied:

$$T_{ft} = \sum_{t=0}^{T_t} \varphi(t)\Delta T, \tag{19}$$

where ΔT is the sample time in the discrete data, and

$$\varphi(t) = \begin{cases} 1 & \text{if } P_T^{av}(t) < P_T^{req}(t) \\ 0 & \text{otherwise} \end{cases}. \tag{20}$$

The total available power in the DC bus is

$$P_T^{av}(t) = N_w \eta_{AD} P_{w,un}^{av}(t) + N_{PV}\eta_{DD} P_{PV,un}^{av}(t) + N_{FC}\eta_{DD} P_{FC,un}^{av}(t) + N_b \eta_{DD} P_{b,un}^{dsch}(t), \tag{21}$$

where $P_{w,un}^{av}(t)$ is the power generated by one wind unit, $P_{PV,un}^{av}(t)$ is the power generated by one solar unit, $P_{FC,un}^{av}(t)$ is the power generated by one PEM fuel cell module, $P_{b,un}^{dsch}(t)$ is the battery discharge power, N_w is the number of wind units, N_{PV} is the number of solar units, N_{FC} is the number of fuel cell units, and N_b is the number of battery modules. On the other hand, the total power required in the DC bus is

$$P_T^{req}(t) = \frac{1}{\eta_{DA}} P_L^{req}(t) + P_h^{req}(t), \tag{22}$$

where $P_h^{req}(t)$ is the required power by the heater when the reformer-fuel cell system is operating.

The problem of sizing the components of the system can be written as follows:

$$\begin{aligned} &\min_{\mathbf{x}} \{C_T(\mathbf{x}) + \rho C_{Et}(\mathbf{x}, SOC_i, EMS)\} \\ \text{subject to}: \quad &\mathbf{x}^{min} \leq \mathbf{x} \leq \mathbf{x}^{max} \\ &LPSP(\mathbf{x}) \leq LPSP_a \end{aligned} \tag{23}$$

Equation (23) represents a multiobjective optimization where the functional cost consists of two competing components: the total capital cost of the system $C_T(\mathbf{x})$ and the ethanol consumption $C_{Et}(\mathbf{x},SOC_i,EMS)$. The total capital cost is the sum of the initial investment cost, maintenance cost, and the replacement cost. The maintenance cost and the replacement cost are considered for a period of time equal to the lifetime of the system. The ethanol consumption C_{Et} represents the cost of the consumed ethanol along the lifetime. The lifetime of the system is assumed to be 20 years. The weighting factor called ρ allows directing the relevance towards some of those components. In Ref. [15], only the cost $C_T(\mathbf{x})$ was considered.

The vector $\mathbf{x} = [N_w,N_{PV},N_b,N_{FC}]$ groups together the integer decision variables related to the number of wind turbines, PV panels, batteries, and fuel cells, respectively. The parameter called SOC_i defines the initial state of charge in the battery bank and the acronym EMS shows that the ethanol consumption is strongly related to the energy management strategy used. The constraints in (23) define the searching space via the lower and upper bounds: $\mathbf{x}^{min} = [\mathbf{x}_w^{min}, \mathbf{x}_{PV}^{min}, \mathbf{x}_b^{min}, \mathbf{x}_{FC}^{min}]$ and $\mathbf{x}^{max} = [\mathbf{x}_w^{max}, \mathbf{x}_{PV}^{max}, \mathbf{x}_b^{max}, \mathbf{x}_{FC}^{max}]$ and guarantee the feasibility of the solution by using the loss of power supply probability concept, $LPSP(\mathbf{x})$.

Because of the deep interrelation between the sizing and the EMS, we propose a methodology for the system design that unifies the two tasks. This is a significant improvement from the methodology presented in Ref. [15], where the sizing was addressed separately from the EMS. The unified methodology is based on genetic algorithms, as explained below.

Algorithm 1. GA-based stochastic global search

1 **Initialization:** $j = 0$, setting n_i, n_g, n_s, p_c, p_m, n_c, and $\mathbf{P}_j = [\mathbf{C}_1^T, \ldots, \mathbf{C}_{n_i}^T]^T_{n_i \times n_c}$ (initial random population);
2 **while** (*termination criterion is false*) **do**
3 **Fitness evaluation:** evaluate $f(\mathbf{C}_i)$ for each individual $\mathbf{C}_i$ from the current population set $\mathbf{P}_j$. The best individual is stored in the best population set $\mathbf{P}_b$ and its value in the vector $\mathbf{F}$;
4 **Selection:** the n_s best individuals are selected using their relative fitness values and stored in $\mathbf{P}_s$. *The* $n_i - n_s$ remaining individuals are discarded;
5 **Recombination:** the individuals in $\mathbf{P}_s$ are recombining by the crossover operator and stored in $\mathbf{P}_r$;
6 **Mutation:** the recombined individuals in $\mathbf{P}_r$ suffer the mutation process and new genetic structures are obtained and stored in $\mathbf{P}_m$;

Table 5 – GA parameter settings.

n_c	n_i	n_g	n_s	p_c	p_m	Selection	Crossover
15	100	30	$n_i/2$	0.7	$0.7/n_c$	roulette-wheel	double-point
n_{cw}	n_{cPV}	n_{cb}	n_{cFC}	ρ	$\mathbf{x}^{min}$	$\mathbf{x}^{max}$	$LPSP^{min}$
3	5	4	3	[1,100]	[1,1,1,1]	[5,30,10,5]	5%

7 **Merging:** $j = j+1$ and both selected and mutated populations are merging together to give the next generation of individuals, $\mathbf{P}_j = [\mathbf{P}_s^T, \mathbf{P}_m^T]^T$;
8 **end**

Result: the best population set $\mathbf{P}_b(j \times n_c)$ and the fitness profile $\mathbf{F}(j \times 1)$

4.1. *Design methodology based on genetic algorithms*

Genetic algorithms (GA) represent a well-known methodology to perform a stochastic global search (optimization) by simulating the metaphor of the real biological evolution. Mainly, the GA operate on a population of individuals (potential solutions) which are evaluated, selected, merged, mate, and mutate (operators borrowed from natural genetics) along the generations in order to find the best population according to some particular environment (fitness function) [19].

The individuals, $\mathbf{C}_i = [c_1^i, \ldots, c_{n_c}^i]$, are encoded as strings (chromosomes) composed over some particular alphabet. These decision variables can be evaluated considering some performance or fitness function, $f(\mathbf{C}_i)$ which establishes the basis for pairs selection of individuals that will be mated together during reproduction phase. In this stage, each individual is assigned to a fitness value derived from this objective function and the selection over the population is made with a determined probability according to their relative fitness. Thus, the recombination process is carried out to produce the next generation.

The classical steps involved in any GA-based optimization methodology are shown in Algorithm 1. The initialization phase summarizes all the data required for starting the algorithm: the initial population $\mathbf{P}_0$ (where n_i individuals with length n_c are generated randomly), the maximum allowed generation n_g, the amount of individuals to be selected $n_s = n_i/2$, and the reproduction and mutation probabilities p_c and p_m, respectively. The first evaluation is the criterion for stopping the overall procedure, i.e. the maximum allowed generations.

Considering the definitions previously introduced and the required searching space, a binary representation is selected in this work for the integer decision variable $\mathbf{x}$. Hence, the vector $\mathbf{x}$ is represented as $\mathbf{C}_i = [c_1^i, \ldots, c_{n_c}^i]$, where $c_j^i \in \{0,1\}$ with $j = 1,\ldots,n_c$ and $i = 1,\ldots,n_i$. Indeed, the following parametrization is suggested:

$$\mathbf{C}_i = [\mathbf{C}_i^w, \mathbf{C}_i^{PV}, \mathbf{C}_i^b, \mathbf{C}_i^{FC}], \tag{24}$$

with

$$\mathbf{C}_i^w = [c_1^{wi}, \ldots, c_{n_{cw}}^{wi}], \mathbf{C}_i^{PV} = \left[c_1^{PVi}, \ldots, c_{n_{cPV}}^{PVi}\right], \mathbf{C}_i^b = \left[c_1^{bi}, \ldots, c_{n_{cb}}^{bi}\right], \mathbf{C}_i^{FC} = \left[c_1^{FCi}, \ldots, c_{n_{cFC}}^{FCi}\right] \tag{25}$$

Each subchromosome has a fixed length, n_{cw}, n_{cPV}, n_{cb}, and n_{cFC}, which are defined properly for covering the required searching space $[\mathbf{x}_w^{min}, \mathbf{x}_w^{max}]$, $[\mathbf{x}_{PV}^{min}, \mathbf{x}_{PV}^{max}]$, $[\mathbf{x}_b^{min}, \mathbf{x}_b^{max}]$, and $[\mathbf{x}_{FC}^{min}, \mathbf{x}_{FC}^{max}]$, respectively. The size of the final chromosome in (24) is $n_c = n_{cw}+n_{cPV}+n_{cb}+n_{cFC}$.

Considering this binary parametrization of the decision variables ($\mathbf{x}$) and the parameters set shown in Table 5, the problem defined in (23) can be rewritten to be solved via GA as:

$$\begin{aligned} &\min_{\mathbf{C}_i}\{C_T(\mathbf{x}(\mathbf{C}_i)) + \rho C_{Et}(\mathbf{x}(\mathbf{C}_i), SOC_i, EMS)\} \\ \text{subject to}: \quad &\mathbf{C}_i = [\mathbf{C}_i^w, \mathbf{C}_i^{PV}, \mathbf{C}_i^b, \mathbf{C}_i^{FC}] \\ &\mathbf{x}(\mathbf{C}_i) = T_{bd}(\mathbf{C}_i) \\ &\mathbf{x}^{min} \le \mathbf{x}(\mathbf{C}_i) \le \mathbf{x}^{max} \\ &LPSP(\mathbf{x}(\mathbf{C}_i)) \le LPSP^{min} \end{aligned} \tag{26}$$

where $T_{bd}(\mathbf{C}_i)$ is a translation function which performs two basic operations: 1- divides the current chromosome for obtaining the subindividuals $\mathbf{C}_i^w$, $\mathbf{C}_i^{PV}$, $\mathbf{C}_i^b$, and $\mathbf{C}_i^{FC}$, and 2- performs a binary to decimal translation for each subindividual and recovers the original $\mathbf{x}=[N_w,N_{PV},N_b,N_{FC}]$. The optimization problem stated in (26) is solved by using a GA routine as shown

Table 6 – Optimal solutions given by the GA-based approach.

	Costs		$\mathbf{x}$				$\mathbf{C}_o$														
							$\mathbf{C}_o^w$			$\mathbf{C}_o^{PV}$					$\mathbf{C}_o^b$				$\mathbf{C}_o^{FC}$		
ρ	C_T	C_{Et}	N_w	N_{PV}	N_b	N_{FC}															
1	106,128	6289.39	1	1	1	4	0	0	1	0	0	0	0	1	0	0	0	1	1	0	0
10	106,128	6289.39	1	1	1	4	0	0	1	0	0	0	0	1	0	0	0	1	1	0	0
20	106,128	6289.39	1	1	1	4	0	0	1	0	0	0	0	1	0	0	0	1	1	0	0
30	133,701	5180.25	2	2	1	4	0	1	0	0	0	0	1	0	0	0	0	1	1	0	0
40	179,373	3844.16	3	6	1	4	0	1	1	0	0	1	1	0	0	0	0	1	1	0	0
50	276,989	1696.84	3	18	5	3	0	1	1	1	0	0	1	0	0	1	0	1	0	1	1
60	325,922	797.92	2	29	7	2	0	1	0	1	1	1	0	1	0	1	1	1	0	1	0
70	325,922	797.92	2	29	7	2	0	1	0	1	1	1	0	1	0	1	1	1	0	1	0
80	357,605	342.18	3	30	9	1	0	1	1	1	1	1	1	0	1	0	0	1	0	0	1
90	357,605	342.18	3	30	9	1	0	1	1	1	1	1	1	0	1	0	0	1	0	0	1
100	357,605	342.18	3	30	9	1	0	1	1	1	1	1	1	0	1	0	0	1	0	0	1

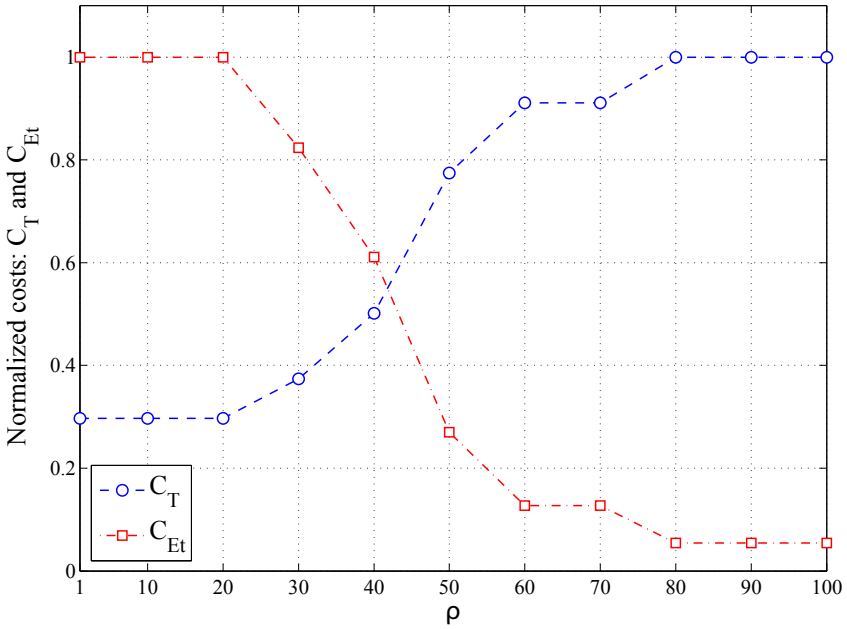

Fig. 3 – Pareto of normalized functional components.

in Algorithm 1 where the mutation phase is performed via four parallel operators. One for each subchromosome instead of mutating the entire individual. This new mutation procedure guarantees diversity (exploration) in the solution, without affects the convergence of the algorithm (exploitation), by using a fixed mutation probability. Some analysis and results about the recombination operators and the optimal/adaptive mutation rates in GA can be found in Refs. [20,21].

The design process is performed using historical hourly data of solar radiation (accessed from Ref. [22]), wind speed and ambient temperature (accessed from Ref. [23]) over the year 2011. The data chosen to be the load requirement for the hybrid renewable system is a scaled version of data accessed from Ref. [24].

The main results from the GA-based optimization approach are shown in Table 6. In this case, eleven optimal solutions are explored by modifying the weighting factor ρ in the range $[1, 100]$. The basic idea here is analyzing how the optimal solutions evolve when the relevance between the investment, maintenance, and replacement costs (C_T) and ethanol consumption (C_{Et}) is modified in the original fitness function. In this table can be observed the optimal solutions obtained from the decision variable space $\mathbf{C}_o$ and its corresponding decimal translation $\mathbf{x}$.

Because C_T and C_{Et} have competing objectives, it is more useful to analyze their evolution through the Pareto chart shown in Fig. 3. In this case, the profiles are normalized according to the maximum value. When the weighting factor has low values, i.e. <40, the search is mainly focused on minimizing the C_T cost regardless of the evolution in C_{Et}. In this context, the feasible optimal solutions basically evolve to designs with very low devices indicating clearly low investment, maintenance, and replacement costs. On the other hand, when $\rho > 40$ the ethanol consumption is strongly penalized and less consideration is required on the C_T profile. Thus, the feasible optimal solutions evolve toward designs which prioritize the inclusion of renewable energy sources regardless of their costs. The trade-off solution suggested from the Pareto chart is $\rho = 40$. However, Fig. 3 should be considered only as a sizing tool since that the final decisions about the hybrid system design depend on several factors such as investment, physical space, bio-ethanol sources, etc.

On the other hand, the optimal values for the functional cost in (26) along the range selected for ρ. It is clear that when the weighting factor increases the profile of $C_T + \rho C_{Et}$ presents minimal variations of its optimal values. This fact indicates

Table 7 – Parameters used in the EMS validation.

Parameter	Description	Value
SOC_b^{min}	Minimum state of charge	40%
SOC_b^{max}	Maximum state of charge	100%
ΔSOC_b^{thr}	Threshold of the state of charge	20%
Δp^{thr}	Threshold of the load current	1000 W

Table 8 – Validation results for some different values of ρ

ρ	N_w	N_{PV}	N_b	N_{fc}	$LPSP$ [%]	C_{Et} [$]	C_T [$]
1	1	1	1	4	3.9	6123.4	106,128
10	1	1	1	4	3.9	6123.4	106,128
20	1	1	1	4	3.9	6123.4	106,128
30	2	2	1	4	2.9	4888.0	133,701
40	3	6	1	4	3.4	3524.1	179,373
50	3	18	5	3	4.2	1514.0	276,989
60	2	29	7	2	4.3	741.6	325,922
70	2	29	7	2	4.3	741.6	325,922
80	3	30	9	1	4.1	301.9	357,605
90	3	30	9	1	4.1	301.9	357,605
100	3	30	9	1	4.1	301.9	357,605

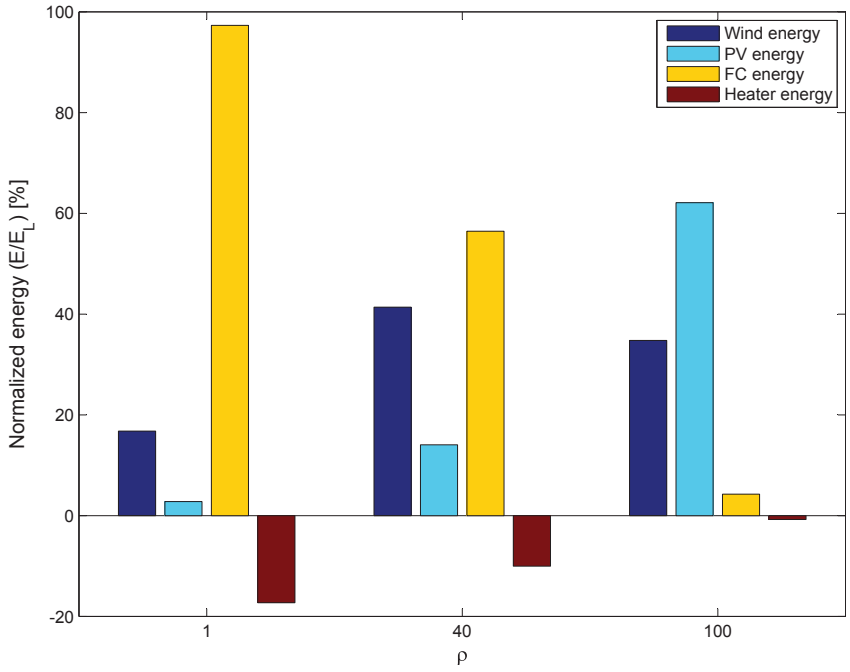

Fig. 4 – Energy balance along a year for different values of ρ.

that there are several solutions with very close fitness function values when $60 \leq \rho \leq 100$, so any searching process becomes a very complex and difficult task.

In this work, the GA-based search is implemented by using the GA toolbox developed by Ref. [19] for the Matlab environment (http://codem.group.shef.ac.uk/index.php/ga-toolbox). On the other hand, some applications of GA to complex binary/combinatorial problems in the process control area can be found in Refs. [25–27].

5. Results

In this Section, the methodology for optimal sizing, presented in Section 4, is validated. For this purpose, a new historic data set of atmospheric conditions (wind speed, ambient temperature and solar insolation), corresponding to the year 2012, was collected. The hybrid renewable energy system, designed with different values of the parameter ρ (shown in Table 6) is

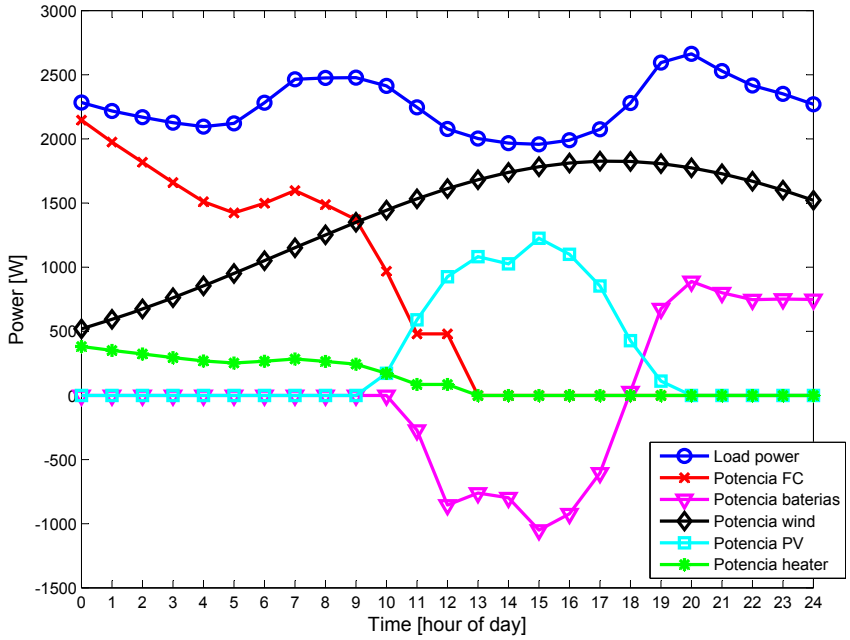

Fig. 5 – Power split between the power sources to meet the load.

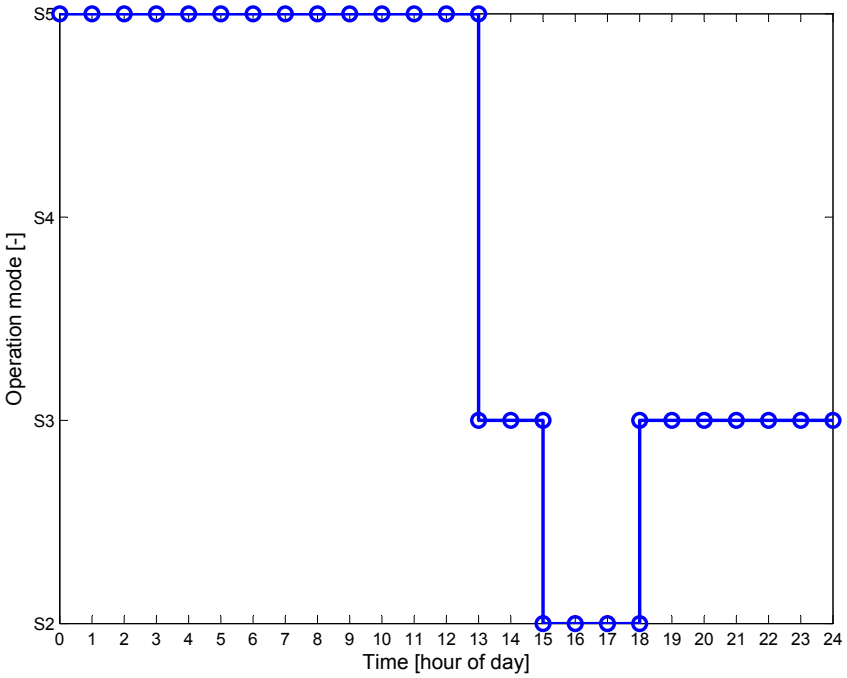

Fig. 6 – Operation mode of the EMS.

simulated with the model implemented in Matlab/Simulink, according to the description in Section 2, using this new historic data set. The system is operated using the EMS enunciated in Section 3 with the parameters presented in Table 7. The simulation results indicates that all the design met the *LPSP* requirement, as it shown in Table 8 for some values of ρ, together with the corresponding costs C_{Et} and C_T.

Fig. 4 shows the energy balance along a year of each component except the battery (which serves as a power buffer) for 3 different values of ρ. The energies are normalized with respect to the load energy: E_i/E_L. E_i is the energy of the i power source over the year, where the index i is either wind, PV, FC or heather. E_L is the annual energy demanded by the load. Note that the heater energy is negative because this energy is consumed from the DC bus. This figures show that the methodology provides also a flexibility degree to accommodate the design to different scenarios, according to the availability of renewable resources and bioethanol. Thus,

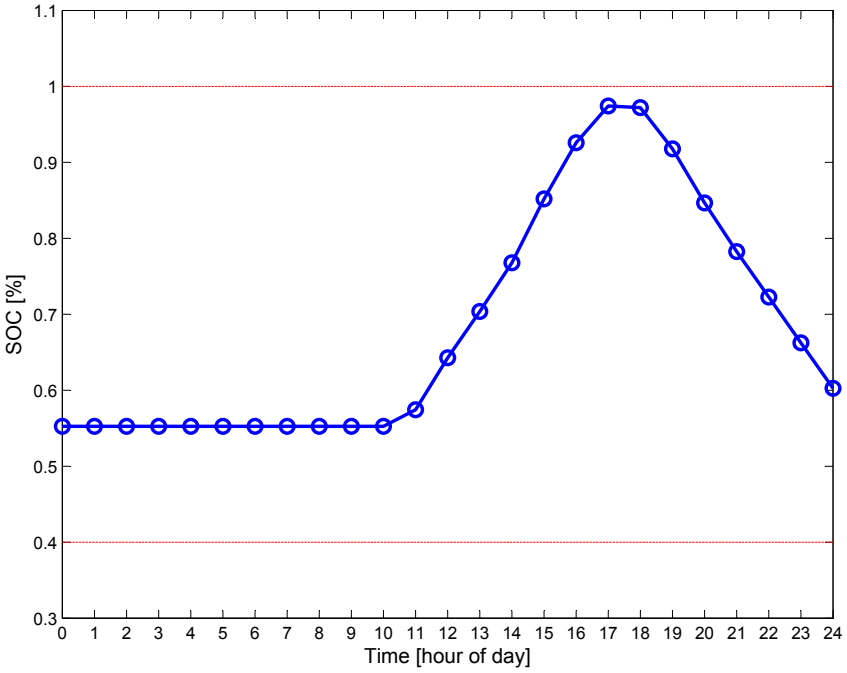

Fig. 7 – State of charge (SOC) of the battery bank.

selecting an appropriate value of ρ, it is possible to design different hybrid systems: with low ρ values the bioethanol use is predominant while, on the contrary, with high ρ values the use of renewable energy is prioritized.

To illustrate the behavior of the system operated by the EMS, it is shown the temporal evolution of the system with $\rho = 40$ ($N_w = 3$,$N_{PV} = 6$,$N_b = v1$,$N_{fc} = 4$) along a given day of the validation data set: Fig. 5 shows the power split, Fig. 6 shows the operation mode, while Fig. 7 shows the SOC_b. It can be seen that the system satisfactorily meets the load requirement despite during most of the time the wind-solar generation is small. The operation mode changes depending on the available power, the demand and the SOC_b. As a result of the operation sequence, the SOC_b evolves within the upper and lower limits.

It can be seen from the figures that the wind and solar system are kept in continuous operation, at maximum capacity, and the load is mainly supported by these systems. The battery makes an important job, meeting the high demands, or when environmental resources are too low. On the other hand, the PEM fuel cell is operated to supply the high demand periods and when the SoC_b is low, allowing to recover the battery charge for its utilization a posteriori. From these observations it can be inferred that the wind-solar system is in charge of the base operation, while the battery adjusts the delivered power in accordance with the demand. Moreover, the FC is in charge of securing the sustainability of the system, maintaining the battery in adequate conditions, supplying the periods of bad weather conditions (including maintenance work), and fundamentally assuring the satisfaction of the demand when it is too high for the rest of the renewable hybrid system.

6. Conclusions

The concept of a hybrid energy system based on multiple renewable power sources, hydrogen production from bioethanol and energy storage systems, is very appealing due to its flexibility, sustainability and energy management capabilities. In order to provide uninterrupted power supply, the reformer-fuel cell system performs a fundamental role. It is worth noting that the presence of the bioethanol-fuel cell system allows to decrease the sizing of the other components, guaranteeing its operability even against adverse conditions. This is because of the inclusion of a chemical energy reserve that is environmentally friendly such as the bioethanol. This paper has proposed a design methodology, integrated with the energy management strategy, for the hybrid energy system. Although the study is intended for one particular system, the proposed design methodology is applicable for other hybrid systems with multiple renewable sources. The proposed methodology uses long term data (1 year) of meteorological conditions (wind speed, ambient temperature and insolation) and power demand, to determine the number of system components to meet a given *LPSP* requirement with the lowest cost and bioethanol consumption. The validation of the designs using a different weather data set shows the robustness of the proposed methodology. The methodology provides also a flexibility to accommodate the design to different scenarios, according to the availability of renewable resources and bioethanol. To conclude, it is aimed to contribute to the literature on design of hybrid renewable energy systems with a new perspective on optimum sizing.

Acknowledgments

The authors thank the financial support of CONICET (National Scientific and Technical Research Council), UNR-FCEIA (Rosario National University), and ANPCYT PICT 2009-0017 (Agencia Nacional de Promoción Científica y Técnica) from Argentina. The authors also acknowledge the support of UTN-FRRo.

Nomenclature

Acronyms

BRS	bioethanol reformer system
CSTR	continuously stirred tank reactors
EMS	energy management strategy
ESR	ethanol steam reformer
GA	genetic algorithm
LPSP	loss of power supply probability
PEM	Polymer Electrolyte Membrane
PV	photovoltaic
WGS	water gas shift reactors

Variables

A	swept blade area of the wind turbine
A_c	cell deviation from the ideal p-n junction characteristic
C_{PV}	initial cost of PV panels
C_b^*	battery capacity
C_C	initial cost
C_f	design constant of the blades
C_M	maintenance cost
C_P	efficiency of the turbine
C_R	replacement cost
E	energy
E_{go}	band-gap energy of the semiconductor used in the photovoltaic cell
I_{or}	reverse saturation current at the reference temperature
I_{ph}	photovoltaic cell current under a given insolation
I_{PV}	photovoltaic current
I_{sc}	short-circuit photovoltaic cell current
I_o	current on the output terminal of the PV power converter
I_{rs}	photovoltaic cell reverse saturation current
J	cost functional
K	Boltzman constant
K_I	short-circuit current temperature coefficient
$LPSP_a$	allowed loss of power supply probability
N_b	number of batteries
N_{FC}	number of fuel cells
N_{PV}	number of PV panels
N_w	number of wind turbines
P	power

P_{FC}	fuel cell power
P_b	battery power
P_h	heater power
P_L	load power
P_w	wind turbine power
q	charge of an electron
r	radius of the blades
R_{int}	battery internal resistance
S	set of nodes in the statechart
s_0	initial state in the statechart
SOC_b	battery state of charge
T	temperature
T_{ft}	power failure time
T_{op}	operation time
T_t	total time
v	wind velocity
V_{bus}	bus voltage
V_{oc}	battery open circuit voltage
V_b	battery bank voltage
$\mathbf{x}$	vector of decision variables

Greek Symbols

β	blade angle
ΔT	sampling time
δ	function that maps states and input events to states in the statechart
λ	tip speed ratio
ω_m	speed angle of the turbine shaft
ρ	penalization term
ρ_a	air density
Σ	set of possible input events in the statechart

REFERENCES

[1] Feroldi D, Serra M, Riera J. Energy management strategies based on efficiency map for fuel cell hybrid vehicles. J Power Sources 2009;190(2):387–401.

[2] Valenciaga F, Puleston P, Battaiotto P, Mantz R. Passivity/sliding mode control of a stand-alone hybrid generation system. IEE Proc Control Theory Appl 2000;147(6):680–6.

[3] Lei Y, Mullane A, Lightbody G, Yacamini R. Modeling of the wind turbine with a doubly fed induction generator for grid integration studies. IEEE Trans Energy Convers 2006;21(1):257–63.

[4] Boukhezzar B, Lupu L, Siguerdidjane H, Hand M. Multivariable control strategy for variable speed, variable pitch wind turbines. Renew Energy 2007;32(8):1273–87.

[5] Boukhezzar B, Siguerdidjane H. Nonlinear control of variable speed wind turbines for power regulation. In: Control applications, 2005. CCA 2005. Proceedings of 2005 IEEE Conference on. IEEE; 2005. pp. 114–9.

[6] Valenciaga F, Puleston PF, Battaiotto PE. Power control of a photovoltaic array in a hybrid electric generation system using sliding mode techniques. Control Theory Appl IEEE Proc Nov 2001;148(6):448–55.

[7] Larminie J, Dicks A. Fuel cell systems explained. 2nd ed. Wiley and Sons; 2003.

[8] Francesconi Javier A, Mussati Miguel C, Mato Roberto O, Aguirre Pio A. Analysis of the energy efficiency of an integrated ethanol processor for Pem fuel cell systems. J Power Sources 2007;167(1):151–61.

[9] Johnson VH. Battery performance models in advisor. J Power Sources 2002;110(2):321–9.

[10] Valenciaga F, Puleston PF. Supervisor control for a stand-alone hybrid generation system using wind and photovoltaic energy. Energy Convers IEEE Trans 2005;20(2):398–405.

[11] Nieto Degliuomini Lucas, Feroldi Diego, Basualdo Marta. Hydrogen production based on bio-ethanol and solar energy for feeding Pem fuel cells. In: 20th Mediterranean conference on control and automation (2012) 2012. pp. 1183–8.

[12] Qi W, Liu J, Chen X, Christofides PD. Supervisory predictive control of standalone wind/solar energy generation systems. Control Syst Technol IEEE Trans 2011;19(1):199–207.

[13] Zhou K, Ferreira JA, De Haan SWH. Optimal energy management strategy and system sizing method for stand-alone photovoltaic-hydrogen systems. Int J Hydrogen Energy 2008;33(2):477–89.

[14] Ipsakis D, Voutetakis S, Seferlis P, Stergiopoulos F, Elmasides C. Power management strategies for a stand-alone power system using renewable energy sources and hydrogen storage. Int J Hydrogen Energy 2009;34(16):7081–95.

[15] Feroldi Diego, Nieto Degliuomini Lucas, Basualdo Marta. Energy management of a hybrid system based on wind-solar power sources and bioethanol. Chem Eng Res Des 2013;91(8):1440–55.

[16] Schneider Fred B. The state machine approach: a tutorial. Springer; 1990.

[17] Rajkumar RK, Ramachandaramurthy VK, Yong BL, Chia DB. Techno-economical optimization of hybrid pv/wind/battery system using neuro-fuzzy. Energy 2011;36(8):5148–53.

[18] Yang HX, Lu L, Burnett J. Weather data and probability analysis of hybrid photovoltaic–wind power generation systems in hong kong. Renew Energy 2003;28(11):1813–24.

[19] Chipperfield A, Fleming P, Pohlheim H, Fonseca C. Genetic algorithm toolbox. for use with Matlab, vol. 44. University of Sheffield; 1994. pp. 5645–59. http://codem.group.shef.ac.uk/index.php/ga-toolbox.

[20] Ochoa G, Harvey I, Buxton H. On recombination and optimal mutation rates. In: Proceedings of genetic and evolutionary computation conference (GECCO-99) 1999. pp. 488–95.

[21] Uyar S, Eryigit G, Sariel S. An adaptive mutation scheme in genetic algorithms fastening convergence to the optimum. In: Proceedings of 3rd APIS: Asian Pacific International Symposium on Information Technologies 2004.

[22] HomerEnergy. Energy modeling software for hybrid renewable energy systems. Available online; September 2012 [accessed on September 2012].

[23] Meteored. Global climate, climatic data worldwide. Available online; September 2012 [accessed on September 2012].

[24] Ercot. Ercot – hourly load data archives. Available online; May 2013 [accessed on May 2013].

[25] Molina G, Zumoffen D, Basualdo M. Plant-wide control strategy applied to the tennessee eastman process at two operating points. Comput Chem Eng 2011;35:2081–97.

[26] Nieto Degliuomini L, Zumoffen D, Basualdo M. Plant-wide control design for fuel processor system with PEMFC. Int J Hydrogen Energy 2012;37(19):14801–11.

[27] Zumoffen D. Oversizing analysis in plant-wide control design for industrial processes. Comput Chem Eng 2013;59:145–55.